

# Boosting Diffusion-Based Text Image Super-Resolution Model Towards Generalized Real-World Scenarios

Chenglu Pan<sup>1‡</sup> Xiaogang Xu<sup>2\*†</sup> Ganggui Ding<sup>1</sup> Yunke Zhang<sup>2</sup>  
 Wenbo Li<sup>2</sup> Jiarong Xu<sup>3</sup> Qingbiao Wu<sup>1</sup>  
<sup>1</sup>Zhejiang University <sup>2</sup>Huawei Technologies Ltd. <sup>3</sup>Fudan University  
 {chenglupan, dingangui, yunkezhong, qbwu}@zju.edu.cn  
 {xiaogangxu00, fenglinglwb}@gmail.com jiarongxu@fudan.edu.cn

## Abstract

*Restoring low-resolution text images presents a significant challenge, as it requires maintaining both the fidelity and stylistic realism of the text in restored images. Existing text image restoration methods often fall short in hard situations, as the traditional super-resolution models cannot guarantee clarity, while diffusion-based methods fail to maintain fidelity. In this paper, we introduce a novel framework aimed at improving the generalization ability of diffusion models for text image super-resolution (SR), especially promoting fidelity. First, we propose a progressive data sampling strategy that incorporates diverse image types at different stages of training, stabilizing the convergence and improving the generalization. For the network architecture, we leverage a pre-trained SR prior to provide robust spatial reasoning capabilities, enhancing the model’s ability to preserve textual information. Additionally, we employ a cross-attention mechanism to better integrate textual priors. To further reduce errors in textual priors, we utilize confidence scores to dynamically adjust the importance of textual features during training. Extensive experiments on real-world datasets demonstrate that our approach not only produces text images with more realistic visual appearances but also improves the accuracy of text structure.*

## 1. Introduction

Blind text image super-resolution (SR) is a task that aims to restore a high-resolution (HR) image with texts from a given low-resolution (LR) one. This problem is inherently more challenging than natural image SR, as it requires not only reconstructing the visual content but also strictly ensuring that the text’s fidelity and stylistic authenticity are preserved. Errors in the text structure can lead to semantic

misinterpretations, which are unacceptable in the context of restored text images. This challenge is particularly evident when working with Chinese text, where even slight deviations in the stroke patterns of characters can lead to entirely different meanings, making the generated images look unnatural and unrealistic.

Existing SR methods for text images [4, 25–27, 35] leverage text priors to guide the restoration process, incorporating loss functions that enforce correct text structures. While these approaches perform well in many cases, they struggle with images that contain complex strokes or intricate fonts, resulting in inaccurate text feature restoration [47]. Additionally, some methods improve architectures. E.g., MACRONet [21] utilize a codebook to store character codes, which are helpful for generating structural details, and StyleGAN [16] is used to generate aesthetically pleasing text styles. However, these methods still fail when applied to LR images derived from unseen scenarios.

Recently, diffusion models (DM) [11, 32] have shown great promise in image restoration tasks, and researchers have started applying these models to text image SR [31, 47]. These methods leverage the generative capabilities of DMs to restore images by modeling both the realistic image distribution and the underlying text prior. The combination of these two modalities significantly improves image quality compared to earlier methods. However, when dealing with real-world LR images, these methods still face significant challenges, especially when fine-tuning pre-trained models. The errors inherited from the pre-training phase can hinder the model’s ability to adapt to specific downstream tasks, limiting its effectiveness. Moreover, when OCR modules generate erroneous priors for LR images, the resulting super-resolved images may contain inaccurate or nonsensical text, which degrades the quality and clarity.

Moreover, we also observe that when diffusion models are trained solely on real data, they struggle to converge effectively, preventing significant improvements in SR per-

\*Project Lead.

†Corresponding Author.

‡This work is done during the internship of Chenglu Pan at Huawei.



Figure 1. Text image super-resolution results derived by different methods on real-world text images. Our model achieves superior accuracy with zero recognition errors while generating high-resolution text images, ensuring both precision and visual clarity.

formance. Therefore, a dynamic sampling strategy for the real data and synthetic data (e.g., synthesized by BSRGAN [44] and Real-ESRGAN [36]) is required. These shortcomings underline the need for an SR approach that is more adaptable and capable of generalizing to various degradation levels encountered in real-world scenarios.

To address these challenges, we propose a novel solution that enhances the model’s generalization ability through different aspects, including mixed training, new architecture, and confidence scores.

The mixed training aims to stabilize the convergence and improve the generalization ability. We begin by using degraded HR images as input to the model, establishing a strong foundation for text image restoration. Subsequently, we incorporate LR images from real-world scenarios into the training pipeline, enabling the model to adapt to a wide range of degradation types and improving its performance in more varied and realistic conditions. Finally, by progressively incorporating both degraded HR and real-world LR images into the training process, we enhance the model’s capacity to handle diverse real-world conditions, ultimately boosting its accuracy and generalization power.

Additionally, we argue that text image SR requires a more efficient network structure by using a SR-based diffusion rather than the large pre-trained text-to-image models like Stable Diffusion. In this paper, we employ ResShift [43] as an example to provide the SR prior. ResShift is a lightweight model that can be integrated with text modality inputs, enabling superior performance with fewer inference steps. This choice alleviates the challenges of fine-tuning large pre-trained models while maintaining high efficiency in both training and inference. We implement the interac-

tion with text modality via the similar mechanism proposed in DiffTSR [47].

To further enhance the restoration quality, we propose the employment of confidence scores derived from an OCR module. By integrating confidence scores into the interaction with text modality, we can filter out low-confidence predictions and selectively refine only those areas where the model is uncertain. This mechanism helps reduce the occurrence of severe textual distortions by ensuring that the restoration process focuses on refining areas of the image that are more prone to error. As a result, this confidence-based approach helps to preserve text fidelity, ensuring that the final output is both accurate and visually coherent.

By focusing on improving generalization and adaptability, our method offers a robust solution to the challenges faced in text image SR, particularly in real-world scenarios. In summary, our contributions are as follows:

- We introduce a novel mixed training strategy that progressively incorporates both degraded HR and real-world LR images to enhance the model’s generalization ability and improve its performance in diverse text image restoration tasks.
- We reveal that a SR-based lightweight diffusion model is more suitable for text image SR, achieving better results and computational efficiency than the methods using large pre-trained text-to-image models. We further incorporate cross-attention from text priors and a confidence-guided mechanism, effectively enhancing text fidelity and structural consistency in super-resolution.
- We demonstrate, through extensive experiments, that our model outperforms existing methods in the SR task for real-world text images, achieving better generalization

and restoration quality.

## 2. Related Works

**Blind Image Super-Resolution.** Blind image super-resolution aims to recover high-quality images from low-resolution inputs that have undergone complex, unknown degradations in real-world scenarios. Recent advancements in this field have tackled the problem from two primary perspectives: degradation estimation [1, 9, 13, 22, 28, 33] and real-world data synthesis [3, 8, 15, 20, 29, 36, 37, 44]. The former focuses on estimating degradation models from LR images in an unsupervised manner [33], followed by the application of non-blind super-resolution methods. The latter, on the other hand, constructs LR-HR training pairs through a sophisticated degradation process that mimics real-world image deterioration. However, we observe that when it comes to text images, where characters exhibit specific and semantic text styles, relying solely on predefined degradation models is insufficient for achieving optimal restoration performance. Thus, using more advanced models like diffusion is required.

**Diffusion Models.** Inspired by the non-equilibrium thermodynamics theory [14], diffusion model [11, 32] is proposed to model complex distributions and has achieved impressive performance in various generative modeling tasks, including image/video generation [12, 30, 38, 41, 46] and audio synthesis [19]. Diffusion model aims to build the conditional distribution through a Markov Chain, where a sequence of small Gaussian noise is gradually added to the latent vector  $z$  for  $T$  steps, and the sizes of noise are controlled by a variance schedule  $\{\beta_t\}_{t=1}^T$ . Suppose that the latent data distribution is  $q(z)$ , the forward process is:

$$q(z_t|z_{t-1}) = \mathcal{N}(z_t; \sqrt{1 - \beta_t}z_{t-1}, \beta_t\mathbf{I}). \quad (1)$$

By using the reparameterization tricks,  $z_t$  at any timestep  $t$  can be sampled through

$$q(z_t|z_0) = \mathcal{N}(z_t; \sqrt{\bar{\alpha}_t}z_0, (1 - \bar{\alpha}_t)\mathbf{I}), \quad (2)$$

where  $\alpha_t = 1 - \beta_t$  and  $\bar{\alpha}_t = \prod_{k=1}^t \alpha_k$ . Since  $\beta_t$  is small enough, the distribution of reverse  $q(z_{t-1}|z_t)$  is also Gaussian. Therefore the reverse step can also be modeled through a neural network  $\theta$ , denoted as  $p_\theta(z_{t-1}|z_t)$ :

$$p_\theta(z_{t-1}|z_t) = \mathcal{N}(z_{t-1}; \mu_\theta(z_t, t), \tilde{\beta}_t\mathbf{I}), \quad (3)$$

$$\mu_\theta(z_t, t) = \frac{1}{\sqrt{\alpha_t}}(z_t - \frac{1 - \alpha_t}{\sqrt{1 - \bar{\alpha}_t}}\epsilon_\theta(z_t, t)), \quad (4)$$

where  $\tilde{\beta}_t = \frac{1 - \bar{\alpha}_{t-1}}{1 - \bar{\alpha}_t}\beta_t$ ,  $\epsilon_\theta$  is the noise predicted by neural network, and the mean  $\mu_\theta$  is derived through Bayes rules.

Benefiting from the strong power of data distribution modeling of diffusion models, plenty of works [17, 39] also

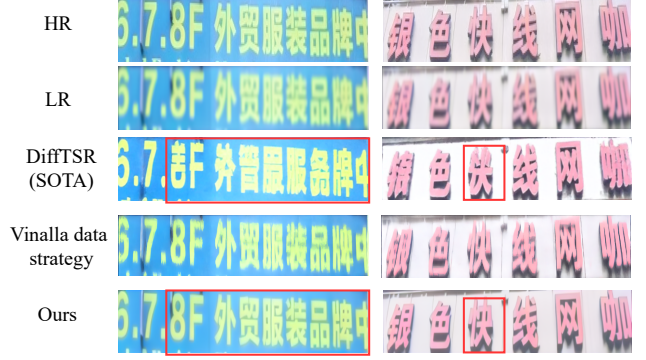


Figure 2. Results when training with only the real-world LR images (vanilla data strategy) and with our data strategy.

achieve impressive performance in image super-resolution via the diffusion prior. However, they still have some failing cases. **Text Image Super-Resolution.** Text image super-resolution aims to enhance the fine details and clarity of text images, with a particular emphasis on improving text readability and recognition accuracy. Recent advances have largely focused on integrating text-specific priors and character structure priors to enhance the performance of text image SR. Specifically, prior works have leveraged text-related information from three primary perspectives: text-aware loss functions [4, 34, 35], text recognition priors [25, 40, 48], and text structure priors [21]. These approaches have demonstrated that text priors are essential for improving the structural integrity of text in the super-resolution process. Despite the effectiveness of these priors, most existing methods fail to fully exploit the available text prior information, often struggling with challenges such as diverse text styles, severe degradation, or intricate strokes. Notably, diffusion-based models have recently been applied to text image SR [31, 47]. In this paper, we propose that a SR-based diffusion prior together with a confident textural prior can achieve better performance and efficiency.

## 3. Methods

### 3.1. Overview

In this paper, we propose a method to estimate the HR image  $x_0$  from the given LR image  $y$ . Our method is inspired by DiffTSR [47] while has some distinct improvements. In our framework, an OCR module and a text diffusion model are also employed to recover the text information from the LR image, and a Mixture of multi-modality module (MoM) is used to facilitate the exchange of information between the image and text features.

This section offers a comprehensive description of our approach. In Section 3.2, we propose a novel data sampling strategy that progressively integrates different types of data throughout the training process. Following that, in Section

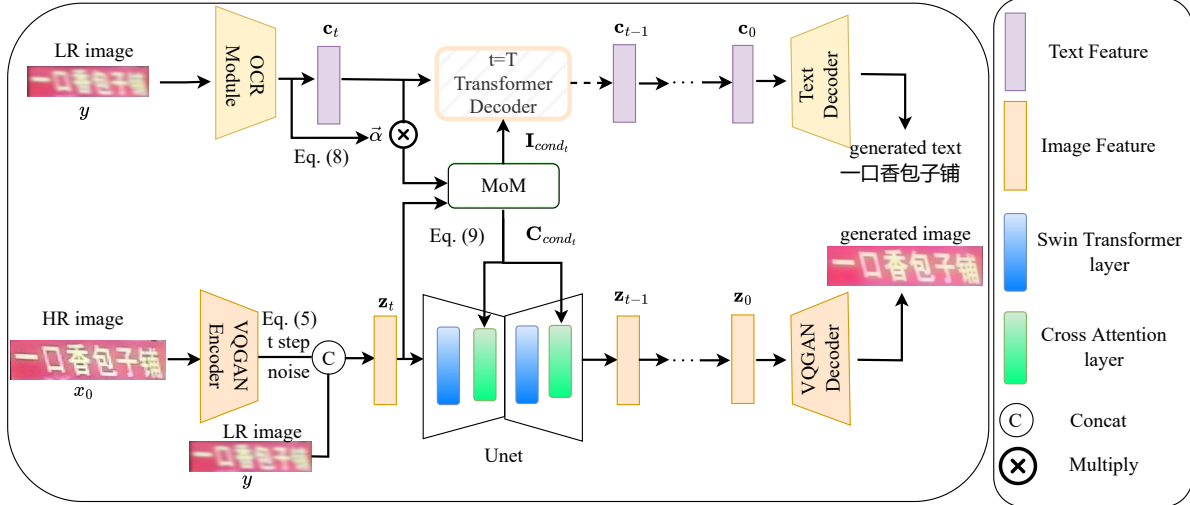


Figure 3. Overview of our framework. Our proposed model uses a Mixture of multi-modality module (MoM) to exchange information between the text diffusion module and the image diffusion module. Before being transmitted to the MoM module, the text feature is multiplied by the confidence score  $\tilde{\alpha}$  to reduce the impact of false generation. Also,  $C_{cond_t}$  generated by the MoM is fused with the image feature via the Cross-attention module in the UNet module, which follows the basic layer in the pre-trained SR network.

3.3, we provide an in-depth explanation of our framework, with an illustrative overview presented in Figure 3. Finally, in Section 3.4, we introduce the loss function that is used to optimize the model.

## 3.2. Data Sampling Strategy During Training

**Our Observations.** In this work, we address a key distinction from previous approaches [21, 31, 47] by focusing on improving the performance towards LR images derived from real-world scenarios. However, directly training the diffusion model with real-world LR images does not yield satisfactory results. As illustrated in Figure 2, when the SR model is trained solely on real-world LR images, the generated outputs show minimal improvement over the input LR image, indicating that the model fails to converge. Moreover, when using degraded HR images as LR inputs, as done in methods like DiffTISR [47], the results are even more problematic—producing false text and suboptimal performance. This highlights the inherent limitations of relying on the sole source of LR images during the training.

**Overview.** In contrast to prior approaches, which predominantly rely on either real-world LR images or degraded HR images, our approach emphasizes a progressive training strategy designed to adapt to the complexities of real-world data. This strategy aims to gradually introduce varying levels of degradation into the training process, allowing the model to better learn from diverse scenarios. By leveraging both degraded HR images and real-world LR images, we enable the model to capture the subtle variations in image quality and text structure that are typical in practical applications. Denoted the degraded HR images as  $\hat{x}_0$ , real-world LR images as  $y$ , and HR images as  $x_0$ .

**Our Implementation.** In our framework, we first conduct the training with the pair of  $\hat{x}_0$  and  $x_0$ , initially building the model’s core SR capabilities. After a few steps of training, we add the LR image  $y$  into training by mixing  $y$  and  $\hat{x}_0$  when constructing the HR-LR pairs, which helps the model to improve the ability of in-domain adaptation. Specifically, during training, given the HR image  $x_0$ , the probabilities of forming an LR-HR pair using  $y$  and  $\hat{x}_0$  are equal.

Furthermore, after a sufficient number of steps with this configuration, we further extend the training process by introducing the degraded LR image, denoted as  $\hat{y}$ . This additional step occurs after learning from  $y$  and  $\hat{x}_0$ , allowing it to gradually adapt to more degradation patterns. By incorporating  $\hat{y}$ , the model is exposed to increasingly complex degradation scenarios, improving its robustness in handling diverse LR inputs.

**Explanation.** This staged approach—starting with degraded HR images, followed by the LR image  $y$ , and then gradually introducing the degraded LR image  $\hat{y}$ —ensures a smooth and gradual progression in the model’s learning process. The model first learns to recover high-resolution details from relatively clean HR images, which serve as a strong prior for the restoration task. As the training progresses, the model is then exposed to the real-world LR image  $y$ , which introduces variability in the data distribution. By incorporating  $y$ , the model starts to develop the capacity for in-domain adaptation, learning to deal with the inherent degradation present in practical scenarios. The introduction of  $\hat{y}$  further enhances the model’s ability to generalize to more out-of-domain and complex degradation patterns. This staged training procedure allows the model to not only preserve the high-frequency details from the HR images but

also adapt effectively to the challenging degradation conditions typical of real-world LR inputs. This is clearly demonstrated in the final row of Figure 2, where the restored images show remarkable enhancement over the baseline, highlighting the effectiveness of our staged approach.

### 3.3. Network Architecture

Since DiffTSR [47] leverages a pre-trained text-to-image diffusion model as the backbone U-Net, it becomes difficult to eliminate the errors inherited from the pre-training phase. We think, in the context of text image SR, leveraging a pre-trained SR model is more essential for restoring the fine details in LR images, while not requiring extensive generative capabilities. A model like ResShift [43], which primarily incorporates self-attention mechanisms through the Swin Transformer architecture, offers robust spatial reasoning capabilities for enhancing image quality. However, it lacks the necessary integration of external textual information, which is crucial for tasks that involve text image restoration.

**Diffusion Procedure.** In this work, we aim to improve text image SR by integrating both SR priors and text-specific priors, addressing the limitations of relying solely on pre-trained text-to-image diffusion priors. While ResShift [43] is an effective SR prior, it is inherently limited in its ability to get textural priors. To overcome this, we introduce a cross-attention layer after each Swin Transformer block, enabling the model to integrate text information directly into the U-Net architecture. This cross-attention mechanism allows the model to not only perform high-quality SR but also perceive the semantic integrity of the text within the images. By doing so, the model gains the ability to restore text images with accurate and coherent textual features, addressing the unique challenges of text image restoration.

The process is carried out in the latent space, where the image  $x_0$  is first mapped into a latent representation  $z_0$  using VQGAN [7]. The forward process is defined as follows:

$$q(z_t|z_{t-1}, y) = \mathcal{N}(z_t; z_{t-1} + \alpha_t e_0, \kappa^2 \alpha_t \mathbf{I}), \quad (5)$$

where  $e_0 = y - x_0$  represents the residual between the LR and HR images, and  $\{\eta_t\}_{t=1}^T$  is the shifting sequence that monotonically increases with timestep  $t$ , with  $\eta_1 \rightarrow 0$  and  $\eta_T \rightarrow 1$ . The hyper-parameter  $\kappa$  controls the noise variance. The reverse distribution can be derived explicitly as [43]:

$$q(z_{t-1}|z_t, y) = \mathcal{N}\left(z_{t-1} \frac{\eta_{t-1}}{\eta_t} z_t + \frac{\alpha_t}{\eta_t} f_\theta(z_t, y, t), \kappa^2 \frac{\eta_{t-1}}{\eta_t} \alpha_t \mathbf{I}\right), \quad (6)$$

where  $f_\theta$  is the deep neural network aiming to predict  $z_0$ . This dual approach—combining ResShift for SR with cross-attention layers for text integration—offers a robust solution to the problem of text image super-resolution. By leveraging both SR priors and text priors, the model can

handle complex text images that feature diverse fonts, structures, and degradation levels. Moreover, this method ensures that fine-grained text details and semantic coherence are maintained during the restoration process.

**Confidence Strategy.** Another challenge occurs when the OCR module generates incorrect predictions for the LR image, as this may impede the image diffusion module’s ability to correct the error, leading to the generation of incorrect characters with entirely different semantic meanings. Therefore, before training the model, we utilize a TransOCR [4] to get the confidence score of the output characters. Specifically, for each character  $i$  in the image, the TranOCR module outputs the prediction  $\hat{i}$  and the confidence score  $\alpha_i$ .  $\alpha_i$  could be denoted as the predicted probability of the character  $i$ . Then the confidence scores of the text image could be formulated as

$$\vec{\alpha} = [\alpha_1, \alpha_2, \dots, \alpha_m], \quad (7)$$

where  $m$  is the length of the text. Then when we convert the text feature to MoM, we could multiply the text feature with the confidence scores of the text image, *i.e.*,

$$[\mathbf{I}_{cond_t}, \mathbf{C}_{cond_t}] = \text{MoM}([z_y, z_t], \vec{\alpha} \cdot c_t, t), \quad (8)$$

where  $z_y$  is the latent representation of LR image  $y$  mapped by VQGAN. The method outlined above leverages the confidence scores from the TransOCR [4] module to adjust the importance of each character during training. By weighting the text features according to their confidence scores, the model can focus more on reliable characters while reducing the impact of erroneous ones.

### 3.4. Loss Function

To optimize the performance of our model, we combine three key loss functions: L1 loss, LPIPS loss, and cross-entropy loss for text recognition. Each of these components is designed to address different aspects of the text image super-resolution task, ensuring both high-quality image restoration and accurate text recovery.

First, the L1 loss is employed to minimize the pixel-wise differences between the generated super-resolved image  $\tilde{x}_0$  and the ground truth HR image  $x_0$ . This term promotes fine-grained restoration by encouraging the model to reduce the absolute pixel differences. Then we incorporate LPIPS [45] loss which enhances the perceptual similarity between the generated and ground truth images, denoted as  $\mathcal{L}_{LPIPS}$ . Unlike L1 loss, which operates at the pixel level, LPIPS captures higher-level semantic differences, improving the visual quality of the output. Finally, the cross-entropy loss  $\mathcal{L}_{CE}$  is introduced to ensure that the text in the generated image is semantically consistent with the ground truth text. This term is computed over the predicted characters and the true characters in the image.

The total loss function is the weighted sum of them:

$$\mathcal{L} = \lambda_1 \mathcal{L}_{L1} + \lambda_2 \mathcal{L}_{LPIPS} + \lambda_3 \mathcal{L}_{CE}, \quad (9)$$

where  $\lambda_1, \lambda_2, \lambda_3$  are the respective hyperparameters controlling the importance of each term.

## 4. Experiments

### 4.1. Experimental Setup

**Datasets** In this work, we mainly focus on the SR of text characters in real-world scenarios as the exploration for complex characters, including Chinese characters. Following [47], we preprocess the image datasets with the following steps: (1) remove the images with a resolution smaller than 64 pixels; (2) only retain the images with a length of texts not larger than 24; (3) only retain the images with a width-to-height greater than 2; (4) resize the image to  $128 \times 512$ . Then, we have over 400K HR text images, and each of these images has a paired LR image. The degradation to generate  $\hat{x}_0$  and  $\hat{y}$  is proposed in BSRGAN [44]. We divide the dataset into training and testing sets, with 80% of the instances divided in the training set and the remaining instances divided in the testing set. We also include the CTR-TSR-Test dataset from [42] for evaluation.

**Evaluation Metrics and Baselines.** To assess the performance of our proposed model, we compare it with several state-of-the-art image SR methods, including general SR approaches (*e.g.*, ESRGAN [36], NAFNet [5]) and recent text image SR techniques (*e.g.*, SRCNN [6], TSRN [35], TSBRN [4], MACRONet [21], DiffTSR [47]). For the baselines without training code, we adopt their released models; for these with training codes, we finetune them with our collected dataset for a fair comparison.

We utilize five evaluation metrics to quantify the effectiveness of these methods. First, we compute the peak signal-to-noise ratio (PSNR) and the learned perceptual image patch similarity (LPIPS) [45]. To further assess the realism of the generated images, we report the Frechet Inception Distance (FID) [10]. For a more specific evaluation of the text fidelity in restored text images, we incorporate word accuracy (ACC) and normalized edit distance (NED) [27]. Notably, we use the pre-trained TransOCR [4, 42] as the text recognition model to compute ACC and NED.

**Implementation Details.** Our method is implemented using PyTorch. All experiments are conducted on a multi-GPU setup with four NVIDIA A100 GPUs, each equipped with 80GB of memory. We set the batch size to 64 and use the Adam optimizer [18] with a learning rate of  $1 \times 10^{-5}$ . In the loss function, the hyperparameters  $\lambda_1, \lambda_2$ , and  $\lambda_3$  are empirically set to 1, 1, and 0.02, respectively.

### 4.2. Quantitative Comparison

We present a quantitative comparison on the synthetic CTR-TSR-Test dataset. As shown in Table 1, our method consistently outperforms all baseline approaches across all evaluation metrics. Specifically, it achieves the highest PSNR, demonstrating its ability to accurately reconstruct text images. Even under significant degradation, such as a  $\times 4$  downsampling factor, our method maintains competitive performance. This can be attributed to the effective incorporation of a learned generative structure prior for each character, which enables robust recovery of text features even from severely degraded inputs. Furthermore, our method excels in both LPIPS and FID, outperforming all baselines. The improved LPIPS suggests that our model preserves more fine-grained structural details, while the lower FID indicates that the generated images are more realistic when compared to real-world examples. In terms of text fidelity, our method also surpasses DiffTSR in both ACC and NED, reflecting its superior ability to maintain the accuracy and structure of the restored text. The inclusion of the confidence score mechanism plays a crucial role, allowing the model to better preserve the integrity of the reliable textual priors during the generation process.

### 4.3. Qualitative Comparison

The qualitative results on the real-world dataset are shown in Figure 4. Our method outperforms all other SR and text super-resolution techniques, including SRCNN [6], NAFNet [5], ESRGAN [36], and the SOTA method DiffTSR [47], in generating high-quality text images. While ESRGAN [36] benefits from GAN-based generation to restore more visually realistic images, some results still exhibit noticeable artifacts, as seen in the second and third results in the third row. Similarly, DiffTSR [47] struggles to preserve realistic image qualities and often generates erroneous text structures.

In contrast, our method, with its strong SR prior and cross-attention mechanism, effectively restores text images with both high style realness and text fidelity. By generalizing well to real-world scenarios, our model produces more accurate and coherent results, surpassing the limitations of existing methods in handling real-world degradation.

### 4.4. Ablation Study

In this subsection, we conduct an ablation study to evaluate the impact of different components in our proposed method. **Remove Cross-attention Module.** For the ‘w/o cross-attention’ experiment where we remove the cross-attention module and perform image recovery using only image features.

As illustrated in the second row of Figure 6, the characters are not well-formed and do not adhere to the correct structure of Chinese characters, leading to visually unpleas-

method	$\times 2$					$\times 4$				
	PSNR $\uparrow$	LPIPS $\downarrow$	FID $\downarrow$	ACC $\uparrow$	NED $\uparrow$	PSNR $\uparrow$	LPIPS $\downarrow$	FID $\downarrow$	ACC $\uparrow$	NED $\uparrow$
ESRGAN	24.75	0.191	9.308	0.8112	0.8239	20.90	0.310	21.86	0.6179	0.6272
SRCNN	23.73	0.338	54.47	0.7856	0.7991	20.74	0.501	116.5	0.6031	0.6160
NAFNet	25.04	0.286	37.42	0.8083	0.8212	21.82	0.447	87.93	0.6451	0.6573
TSRN	20.86	0.392	70.75	0.7805	0.7937	19.41	0.535	137.3	0.6149	0.6267
TBSRN	24.43	0.282	57.61	0.8018	0.8156	21.56	0.442	132.6	0.6360	0.6486
MACRONet	20.77	0.374	94.60	0.6934	0.7068	19.33	0.436	108.5	0.5123	0.5241
DiffTSR	25.08	0.156	5.906	0.8594	0.8718	21.85	0.231	8.482	0.8350	0.8471
Ours	<b>25.34</b>	<b>0.138</b>	<b>3.255</b>	<b>0.8779</b>	<b>0.8913</b>	<b>23.50</b>	<b>0.128</b>	<b>5.583</b>	<b>0.8511</b>	<b>0.8723</b>

Table 1. Quantitative comparison for the synthetic dataset on CTR-TSR-Test [42] with different methods.



Figure 4. Qualitative comparison on the real-world dataset with different methods including SRCNN [6], NAFNet [5], ESRGAN [36], the existing SOTA method DiffTSR [47] and our method for  $\times 4$  super-resolution.

ant results. This is because the model does not incorporate textual priors during the diffusion process, resulting in distorted character shapes and a lack of fidelity in the text.

**Remove Confidence Score.** In the ‘w/o confidence score’ experiment where we omit the confidence score from the OCR model but still use textual features, the performance improves over ‘w/o cross-attention’, resulting in more accurate generated characters that are better aligned with the correct shapes, as shown in the third row of Figure 6. However, some errors still persist. For instance, in the left image, the characters are partially correct but not entirely precise, and in the right image, some entirely incorrect characters are generated. This indicates that without the confidence score mechanism, the model cannot effectively correct errors in the generated text, as it lacks the feedback mechanism needed to refine the output during training.

**Without Progressive Sampling.** In the ‘w/o progressive

sampling’ experiment where we directly use the LR images to train the model, the model is hard to converge, which can be found in the fourth row of Figure 6. Directly training with LR images alone might not provide the model with enough difference between input and ground truth, making it harder for the model to learn fine-grained features necessary for high-quality image restoration.

In our full method, ‘Ours’, which includes both the cross-attention module and the confidence score mechanism, the results improve significantly than these ablation settings. As shown in the fourth row of Figure 6, the generated images exhibit more realistic visual appearances and accurate text structures. The cross-attention mechanism allows the model to better incorporate textual information into the image restoration process, while the confidence score module adjusts the importance of each character during training. This combination results in fewer errors and

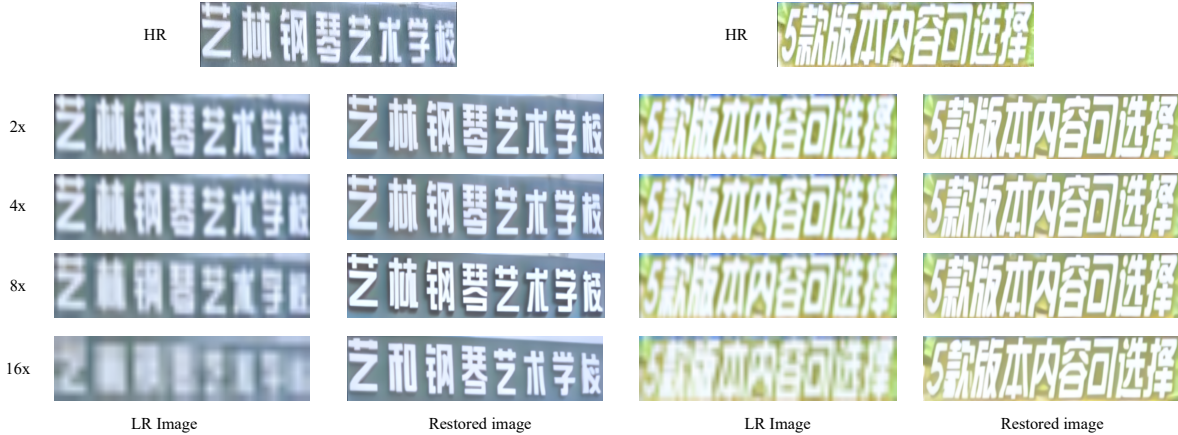


Figure 5. Experiments to validate the robustness of our model towards dealing with various degrees of clarity.



Figure 6. Ablation studies to validate the effectiveness of cross attention part, the confidence score mechanism and the data sampling strategy.

method	x4				
	PSNR $\uparrow$	LPIPS $\downarrow$	FID $\downarrow$	ACC $\uparrow$	NED $\uparrow$
w/o cross-attention	19.54	0.288	25.26	0.7105	0.6934
w/o confidence score	21.83	0.201	7.150	0.7047	0.7136
w/o progressive sampling	19.31	0.345	20.22	0.7415	0.7023
Ours	<b>23.50</b>	<b>0.128</b>	<b>5.583</b>	<b>0.8511</b>	<b>0.8723</b>

Table 2. Ablation Study on CTR-TSR-Test with  $\times 4$  super-resolution to validate the effectiveness of cross attention part, the confidence score mechanism and the data sampling strategy.

better overall text fidelity, demonstrating the effectiveness of both components.

Also, the quantitative results are displayed in Table 2. We can see that by incorporating these components, our method is able to better utilize textual features, leading to more realistic and accurate text restoration. This demonstrates the importance of these three parts.

#### 4.5. Robustness of Our Model

To assess the boundary performance of our model, we introduce a series of degradation operations followed by SR experiments on the degraded images. Specifically, the images are progressively downsampled and upsampled by factors of 2, 4, 8, and 16. The resulting image sequence is shown in Figure 5. As demonstrated, when the scaling factor is below 16, our model excels in restoring the images, producing clear and high-quality results even under significant degradation. When the scaling factor reaches 16, the generated image still retains considerable quality, showing the robustness of our model in handling challenging degradation levels. These results underscore the model’s effectiveness in recovering fine details and maintaining image clarity even at higher scaling factors, which sets it apart from traditional methods. This strong performance suggests that our model could be a promising solution for practical super-resolution tasks, where robustness is highly required.

### 5. Conclusion and Limitation

In this paper, we introduce a novel approach to address the text image super-resolution problem by leveraging a strong super-resolution and reliable textual prior, which enhances the model’s generalization capability. Our method begins with a data sampling strategy that gradually incorporates low-resolution images into the training process. Next, we integrate a powerful SR prior along with a cross-attention layer to incorporate textual features into the UNet architecture. To further improve performance, we employ a confidence score mechanism to minimize errors in the generated images. Extensive experimental results demonstrate that our model outperforms state-of-the-art methods, particularly in terms of style realism and text fidelity.

Despite the promising performance, our model still may produce errors, especially when handling small text in scenes with very low clarity. In future work, we plan to



incorporate reinforcement learning techniques to refine and correct the generated text. Additionally, we aim to replace the OCR module with outputs from multi-modal large language models (MLLMs), which could potentially yield more accurate text outputs from the LR images.

## References

- [1] Sefi Bell-Kligler, Assaf Shocher, and Michal Irani. Blind super-resolution kernel estimation using an internal-gan. *Advances in Neural Information Processing Systems*, 2019. 3
- [2] Kevin Black, Michael Janner, Yilun Du, Ilya Kostrikov, and Sergey Levine. Training diffusion models with reinforcement learning. *arXiv preprint arXiv:2305.13301*, 2023. 12
- [3] Jianrui Cai, Hui Zeng, Hongwei Yong, Zisheng Cao, and Lei Zhang. Toward real-world single image super-resolution: A new benchmark and a new model. In *Proceedings of the IEEE/CVF international conference on computer vision*, 2019. 3
- [4] Jingye Chen, Bin Li, and Xiangyang Xue. Scene text telescope: Text-focused scene image super-resolution. In *Proceedings of the IEEE/CVF Conference on Computer Vision and Pattern Recognition*, 2021. 1, 3, 5, 6
- [5] Liangyu Chen, Xiaojie Chu, Xiangyu Zhang, and Jian Sun. Simple baselines for image restoration. In *European conference on computer vision*, 2022. 6, 7, 13, 14
- [6] Chao Dong, Chen Change Loy, Kaiming He, and Xiaoou Tang. Image super-resolution using deep convolutional networks. *IEEE transactions on pattern analysis and machine intelligence*, 2015. 6, 7, 13, 14
- [7] Patrick Esser, Robin Rombach, and Bjorn Ommer. Taming transformers for high-resolution image synthesis. In *Proceedings of the IEEE/CVF conference on computer vision and pattern recognition*, pages 12873–12883, 2021. 5
- [8] Manuel Fritsche, Shuhang Gu, and Radu Timofte. Frequency separation for real-world super-resolution. In *2019 IEEE/CVF International Conference on Computer Vision Workshop (ICCVW)*, 2019. 3
- [9] Jinjin Gu, Hannan Lu, Wangmeng Zuo, and Chao Dong. Blind super-resolution with iterative kernel correction. In *Proceedings of the IEEE/CVF conference on computer vision and pattern recognition*, 2019. 3
- [10] Martin Heusel, Hubert Ramsauer, Thomas Unterthiner, Bernhard Nessler, and Sepp Hochreiter. Gans trained by a two time-scale update rule converge to a local nash equilibrium. *Advances in neural information processing systems*, 2017. 6
- [11] Jonathan Ho, Ajay Jain, and Pieter Abbeel. Denoising diffusion probabilistic models. *Advances in neural information processing systems*, 2020. 1, 3
- [12] Jonathan Ho, Tim Salimans, Alexey Gritsenko, William Chan, Mohammad Norouzi, and David J Fleet. Video diffusion models. *Advances in Neural Information Processing Systems*, 2022. 3
- [13] Yan Huang, Shang Li, Liang Wang, Tieniu Tan, et al. Unfolding the alternating optimization for blind super resolution. *Advances in Neural Information Processing Systems*, 2020. 3
- [14] Christopher Jarzynski. Equilibrium free-energy differences from nonequilibrium measurements: A master-equation approach. *Physical Review E*, 1997. 3
- [15] Xiaozhong Ji, Yun Cao, Ying Tai, Chengjie Wang, Jilin Li, and Feiyue Huang. Real-world super-resolution via kernel estimation and noise injection. In *proceedings of the IEEE/CVF conference on computer vision and pattern recognition workshops*, 2020. 3
- [16] Tero Karras, Samuli Laine, Miika Aittala, Janne Hellsten, Jaakko Lehtinen, and Timo Aila. Analyzing and improving the image quality of stylegan. In *Proceedings of the IEEE/CVF conference on computer vision and pattern recognition*, 2020. 1
- [17] Bahjat Kawar, Michael Elad, Stefano Ermon, and Jiaming Song. Denoising diffusion restoration models. *Advances in Neural Information Processing Systems*, 2022. 3
- [18] Diederik P Kingma and Jimmy Ba. Adam: A method for stochastic optimization. *arXiv preprint arXiv:1412.6980*, 2014. 6
- [19] Zhifeng Kong, Wei Ping, Jiaji Huang, Kexin Zhao, and Bryan Catanzaro. Diffwave: A versatile diffusion model for audio synthesis. *arXiv preprint arXiv:2009.09761*, 2020. 3
- [20] Xiaoming Li, Chaofeng Chen, Xianhui Lin, Wangmeng Zuo, and Lei Zhang. From face to natural image: Learning real degradation for blind image super-resolution. In *European Conference on Computer Vision*, 2022. 3
- [21] Xiaoming Li, Wangmeng Zuo, and Chen Change Loy. Learning generative structure prior for blind text image super-resolution. In *Proceedings of the IEEE/CVF Conference on Computer Vision and Pattern Recognition*, 2023. 1, 3, 4, 6
- [22] Jie Liang, Hui Zeng, and Lei Zhang. Efficient and degradation-adaptive network for real-world image super-resolution. In *European Conference on Computer Vision*, 2022. 3
- [23] Haotian Liu, Chunyuan Li, Qingyang Wu, and Yong Jae Lee. Visual instruction tuning. *Advances in neural information processing systems*, 2023. 12
- [24] Haoyu Lu, Wen Liu, Bo Zhang, Bingxuan Wang, Kai Dong, Bo Liu, Jingxiang Sun, Tongzheng Ren, Zhuoshu Li, Hao Yang, et al. Deepseek-vl: towards real-world vision-language understanding. *arXiv preprint arXiv:2403.05525*, 2024. 12
- [25] Jianqi Ma, Zhetong Liang, and Lei Zhang. A text attention network for spatial deformation robust scene text image super-resolution. In *Proceedings of the IEEE/CVF Conference on Computer Vision and Pattern Recognition*, 2022. 1, 3
- [26] Jianqi Ma, Shi Guo, and Lei Zhang. Text prior guided scene text image super-resolution. *IEEE Transactions on Image Processing*, 2023.
- [27] Jianqi Ma, Zhetong Liang, Wangmeng Xiang, Xi Yang, and Lei Zhang. A benchmark for chinese-english scene text image super-resolution. In *Proceedings of the IEEE/CVF International Conference on Computer Vision*, 2023. 1, 6
- [28] Shunta Maeda. Unpaired image super-resolution using pseudo-supervision. In *Proceedings of the IEEE/CVF con-*

- ference on computer vision and pattern recognition*, 2020. 3
- [29] Kamyar Nazeri, Eric Ng, Tony Joseph, Faisal Qureshi, and Mehran Ebrahimi. Edgeconnect: Structure guided image inpainting using edge prediction. In *Proceedings of the IEEE/CVF international conference on computer vision workshops*, 2019. 3
- [30] Chitwan Saharia, William Chan, Saurabh Saxena, Lala Li, Jay Whang, Emily L Denton, Kamyar Ghasemipour, Raphael Gontijo Lopes, Burcu Karagol Ayan, Tim Salimans, et al. Photorealistic text-to-image diffusion models with deep language understanding. *Advances in neural information processing systems*, 2022. 3
- [31] Shrey Singh, Prateek Keserwani, Masakazu Iwamura, and Partha Pratim Roy. Dcdm: Diffusion-conditioned-diffusion model for scene text image super-resolution. In *European Conference on Computer Vision*, 2024. 1, 3, 4
- [32] Jascha Sohl-Dickstein, Eric Weiss, Niru Maheswaranathan, and Surya Ganguli. Deep unsupervised learning using nonequilibrium thermodynamics. In *International conference on machine learning*, 2015. 1, 3
- [33] Longguang Wang, Yingqian Wang, Xiaoyu Dong, Qingyu Xu, Jungang Yang, Wei An, and Yulan Guo. Unsupervised degradation representation learning for blind super-resolution. In *Proceedings of the IEEE/CVF conference on computer vision and pattern recognition*, 2021. 3
- [34] Wenjia Wang, Enze Xie, Peize Sun, Wenhai Wang, Lixun Tian, Chunhua Shen, and Ping Luo. Textsr: Content-aware text super-resolution guided by recognition. *arXiv preprint arXiv:1909.07113*, 2019. 3
- [35] Wenjia Wang, Enze Xie, Xuebo Liu, Wenhai Wang, Ding Liang, Chunhua Shen, and Xiang Bai. Scene text image super-resolution in the wild. In *Computer Vision—ECCV 2020: 16th European Conference, Glasgow, UK, August 23–28, 2020, Proceedings, Part X 16*, 2020. 1, 3, 6
- [36] Xintao Wang, Liangbin Xie, Chao Dong, and Ying Shan. Real-esrgan: Training real-world blind super-resolution with pure synthetic data. In *Proceedings of the IEEE/CVF international conference on computer vision*, 2021. 2, 3, 6, 7, 12, 13, 14
- [37] Pengxu Wei, Ziwei Xie, Hannan Lu, Zongyuan Zhan, Qixiang Ye, Wangmeng Zuo, and Liang Lin. Component divide-and-conquer for real-world image super-resolution. In *Computer Vision—ECCV 2020: 16th European Conference, Glasgow, UK, August 23–28, 2020, Proceedings, Part VIII 16*, 2020. 3
- [38] Lemeng Wu, Chengyue Gong, Xingchao Liu, Mao Ye, and Qiang Liu. Diffusion-based molecule generation with informative prior bridges. *Advances in Neural Information Processing Systems*, 2022. 3
- [39] Rongyuan Wu, Lingchen Sun, Zhiyuan Ma, and Lei Zhang. One-step effective diffusion network for real-world image super-resolution. *arXiv preprint arXiv:2406.08177*, 2024. 3
- [40] Xiangyu Xu, Deqing Sun, Jinshan Pan, Yujin Zhang, Hanspeter Pfister, and Ming-Hsuan Yang. Learning to super-resolve blurry face and text images. In *Proceedings of the IEEE international conference on computer vision*, 2017. 3
- [41] Mao Ye, Lemeng Wu, and Qiang Liu. First hitting diffusion models for generating manifold, graph and categorical data. *Advances in Neural Information Processing Systems*, 2022. 3
- [42] Haiyang Yu, Jingye Chen, Bin Li, Jianqi Ma, Mengnan Guan, Xixi Xu, Xiacong Wang, Shaobo Qu, and Xiangyang Xue. Benchmarking chinese text recognition: Datasets, baselines, and an empirical study. *arXiv preprint arXiv:2112.15093*, 2021. 6, 7
- [43] Zongsheng Yue, Jianyi Wang, and Chen Change Loy. Resshift: Efficient diffusion model for image super-resolution by residual shifting. *Advances in Neural Information Processing Systems*, 2024. 2, 5, 11
- [44] Kai Zhang, Jingyun Liang, Luc Van Gool, and Radu Timofte. Designing a practical degradation model for deep blind image super-resolution. In *Proceedings of the IEEE/CVF International Conference on Computer Vision*, 2021. 2, 3, 6
- [45] Richard Zhang, Phillip Isola, Alexei A Efros, Eli Shechtman, and Oliver Wang. The unreasonable effectiveness of deep features as a perceptual metric. In *Proceedings of the IEEE conference on computer vision and pattern recognition*, 2018. 5, 6
- [46] Shu Zhang, Xinyi Yang, Yihao Feng, Can Qin, Chia-Chih Chen, Ning Yu, Zeyuan Chen, Huan Wang, Silvio Savarese, Stefano Ermon, et al. Hive: Harnessing human feedback for instructional visual editing. In *Proceedings of the IEEE/CVF Conference on Computer Vision and Pattern Recognition*, 2024. 3
- [47] Yuzhe Zhang, Jiawei Zhang, Hao Li, Zhouxia Wang, Luwei Hou, Dongqing Zou, and Liheng Bian. Diffusion-based blind text image super-resolution. In *Proceedings of the IEEE/CVF Conference on Computer Vision and Pattern Recognition*, 2024. 1, 2, 3, 4, 5, 6, 7, 11, 13, 14
- [48] Minyi Zhao, Miao Wang, Fan Bai, Bingjia Li, Jie Wang, and Shuigeng Zhou. C3-stsr: Scene text image super-resolution with triple clues. *arXiv preprint arXiv:2204.14044*, 2022. 3

## A. Training Details

**Basic model information.** All the models are trained on the real-world dataset. LR and HR images are resized into  $128 \times 512 \times 3$  and  $32 \times 128 \times 3$ , respectively. Besides, we utilize the TDM and MoM module from [47] and load their pre-trained weights to process the text information and the text diffusion. When training the model, these two modules are frozen. For the Unet module, we utilize the pre-trained weights from the ResShift [43] model. Also, to fuse the textual feature from the MoM module with the image feature, after each basic layers on the ResShift, we insert the Transformer layer for the cross attention module. The Transformer layer is randomly initialized. During training, only the Unet module is updated. Besides, in the modeling of the text sequence, the maximum length of the text is set to 24 and all the characters in the text sequence belong to an alphabet with  $K = 6736$  characters including both Chinese and English characters as well as the numbers and special characters. The total step  $T$  is set to 18.

**Data sampling strategy.** During training, the data sampling strategy is involved. Specifically, for the HR image  $x_0$ , in the first 10K training steps, we only use the degraded image  $\hat{x}_0$  as the LR image, to build the model’s core SR capabilities. In the next 10K training steps, we mix the LR image  $y$  and  $\hat{x}_0$  when constructing the HR-LR pairs to improve the ability of in-domain adaptation. Given the HR image  $x_0$ , the probabilities of using  $y$  and  $\hat{x}_0$  are equal. Finally, in the remaining training rounds, we extend the training process by introducing the degraded LR image  $\hat{y}$  into training. We train the model for 400K steps in total.

**Deviations of Eq. (6).** According to Bayes’s theorem, we have

$$q(z_{t-1}|z_t, z_0, y) \propto q(z_t|z_{t-1}, y)q(z_{t-1}|z_0, y), \quad (10)$$

where

$$q(z_{t-1}|z_t, y) = \mathcal{N}(z_t; z_{t-1} + \alpha_t e_0, \kappa^2 \alpha_t \mathbf{I}), \quad (11)$$

$$q(z_{t-1}|z_0, y) = \mathcal{N}(z_{t-1}; z_0 + \eta_{t-1} e_0, \kappa^2 \eta_{t-1} \mathbf{I}). \quad (12)$$

We focus on the quadratic form in the exponent of  $q(z_{t-1}|z_t, z_0, y_0)$ , *i.e.*,

$$\begin{aligned} & - \frac{(z_t - z_{t-1} - \alpha_t e_0)(z_t - z_{t-1} - \alpha_t e_0)^T}{2\kappa^2 \alpha_t} - \frac{(z_{t-1} - z_0 - \eta_{t-1} e_0)(z_{t-1} - z_0 - \eta_{t-1} e_0)^T}{2\kappa^2 \eta_{t-1}} \\ &= - \frac{1}{2} \left[ \frac{1}{\kappa^2 \alpha_t} + \frac{1}{\kappa^2 \eta_{t-1}} \right] z_{t-1} z_{t-1}^T + \left[ \frac{z_t - \alpha_t e_0}{\kappa^2 \alpha_t} + \frac{z_0 + \eta_{t-1} e_0}{\kappa^2 \eta_{t-1}} \right] z_{t-1}^T + \text{const} \\ &= - \frac{(z_{t-1} - \mu)(z_{t-1} - \mu)^T}{2\lambda^2} + \text{const}, \end{aligned} \quad (13)$$

where

$$\mu = \frac{\eta_{t-1}}{\eta_t} z_t + \frac{\alpha_t}{\eta_t} z_0, \lambda^2 = \kappa^2 \frac{\eta_{t-1}}{\eta_t} \alpha_t, \quad (14)$$

and const denotes the item that is independent of  $z_{t-1}$ . After substituting  $z_0$  with the neural network  $f_\theta(z_t, y, t)$ , this quadratic form induces the Gaussian distribution of Eq. (6).

## B. Procedure of Our Framework

The training and inference procedure of our framework can be summarized in Algorithm 1 and Algorithm 2, respectively.

## C. Efficiency of Our model

To demonstrate the efficiency of our model, we present the total number of parameters and the average inference time per image in Table 3. For the average inference time, we randomly select 100 LR text images from the test set with the size of  $128 \times 512$  as the input. Compared with the state-of-the-art diffusion-based text image SR method, DiffTTSR, our model incorporates a lightweight SR prior, leading to an 82.2% reduction in parameters. Furthermore, our model achieves a 93.4% reduction in inference time, significantly improving efficiency over DiffTTSR. These results highlight the effectiveness of our approach in balancing performance and computational cost.

---

**Algorithm 1** Training of Our Framework

---

```
1: Initialize Training step  $r = 0$ 
2: repeat
3:    $x_0, y, c_0 \sim q(x_0, y, c_0)$ , where  $c_0$  is the ground truth text on  $x_0$ .
4:    $z_0 = E(x_0)$ , where  $E$  is the VQGAN encoder.
5:   Generate  $\hat{x}_0$  and  $\hat{y}$  via the pipeline in ESRGAN [36].
6:   if  $r < 10000$  then
7:      $y' = \hat{x}_0$ 
8:   else if  $10000 \leq r < 20000$  then
9:      $y' = \text{Uniform}(\hat{x}_0, y)$ 
10:  else
11:     $y' = \text{Uniform}(\hat{x}_0, y, \hat{y})$ 
12:  end if
13:   $\bar{\alpha}, c = \text{OCR}(y')$ 
14:   $z_y = E(y')$ 
15:   $\epsilon \sim \mathcal{N}(0, I)$ 
16:   $t \sim \text{Uniform}(\{1, 2, \dots, T\})$ 
17:   $z_t = \sqrt{\bar{\alpha}_t} z_0 + \sqrt{1 - \bar{\alpha}_t} \epsilon$ 
18:   $c_t \sim \mathcal{C}(c_t | \bar{\alpha}_t c_0 + \frac{1 - \bar{\alpha}_t}{K})$ 
19:   $[\mathbf{I}_{cond_t}, \mathbf{C}_{cond_t}] = \text{MoM}([z_y, z_t], \bar{\alpha} \cdot c_t, t)$ 
20:   $\bar{z}_0 = f_\theta(z_t, y, t, \mathbf{C}_{cond_t})$ 
21:   $\bar{x}_0 = D(\bar{z}_0)$ , where  $D$  is the VQGAN decoder.
22:   $\bar{c}_0 = \text{OCR}(\bar{x}_0)$ 
23:   $\mathcal{L} = \lambda_1 \mathcal{L}_{L1}(x_0, \bar{x}_0) + \lambda_2 \mathcal{L}_{LPIPS}(x_0, \bar{x}_0) + \lambda_3 \mathcal{L}_{CE}(c_0, \bar{c}_0)$ 
24:  Take gradient descent on  $\nabla_\theta \mathcal{L}$ 
25: until Converged
```

---

---

**Algorithm 2** Inference of our Framework

---

**Input:** LR image  $y$

**Output:** HR image  $x$

```
1:  $z_y = E(y)$ 
2:  $\epsilon \sim \mathcal{N}(0, I)$ 
3:  $z_T = z_y + \kappa \epsilon$ 
4:  $c_T = \text{OCR}(y)$ 
5: for  $t = T \dots 1$  do
6:    $z \sim \mathcal{N}(0, I)$  if  $t > 1$ , else  $z = 0$ 
7:    $[\mathbf{I}_{cond_t}, \mathbf{C}_{cond_t}] = \text{MoM}([z_y, z_t], \bar{\alpha} \cdot c_t, t)$ 
8:   Sample  $z_{t-1}$  via Eq. (6).
9:    $c_{pred,t} = \tau(c_t, \mathbf{I}_{cond_t}, t)$ , where  $\tau$  is the transformer decoder intended for the text diffusion module.
10:   $\tilde{\pi} = [\alpha_t c_t + \frac{1 - \alpha_t}{K}] \odot [\bar{\alpha}_{t-1} + \frac{1 - \bar{\alpha}_{t-1}}{K}]$ 
11:   $\pi_{post}(c_t, c_{pred,t}) = \frac{\pi}{\sum_{k=1}^K \pi_k}$ 
12:   $c_{t-1} \sim \mathcal{C}(c_{t-1} | \pi_{post}(c_t, c_{pred,t}))$  if  $t > 1$  else  $c_0 \sim \mathcal{C}(c_0 | c_{pred,t})$ 
13: end for
14: return  $x = D(z_0)$  where  $D$  is the VQGAN decoder.
```

---

## D. Future Works

Due to the limited performance of the OCR module, existing methods still make mistakes in the generated images. Therefore, in future work, we plan to incorporate reinforcement learning techniques to refine and correct the generated text, such as DPO [2]. Additionally, we aim to replace the OCR module with outputs from multi-modal large language models (MLLMs) [23, 24], which could potentially yield more accurate text outputs from the LR images.

	# parameters	Inference Time(s)
DiffTSR	874M	25.32
Ours	155M	1.68

Table 3. the total number of parameters and the average inference time on 100 randomly selected LR images of size  $128 \times 512$  for both our model and DiffTSR.

## E. More Visual Results

More visual results are shown in this section for the real-world datasets in Figure 7 and Figure 8. The visual results on the synthetic dataset are shown in Figure 9. Visual results show that our method effectively handle the LR images from the real-world scenarios that contains English letters, numbers and diverse text styles.



Figure 7. Qualitative comparison on the real-world dataset with different methods including SRCNN [6], NAFNet [5], ESRGAN [36], the existing SOTA method DiffTSR [47] and our method for  $\times 4$  super-resolution.



Figure 8. Qualitative comparison on the real-world dataset with different methods including SRCNN [6], NAFNet [5], ESRGAN [36], the existing SOTA method DiffTSR [47] and our method for  $\times 4$  super-resolution.

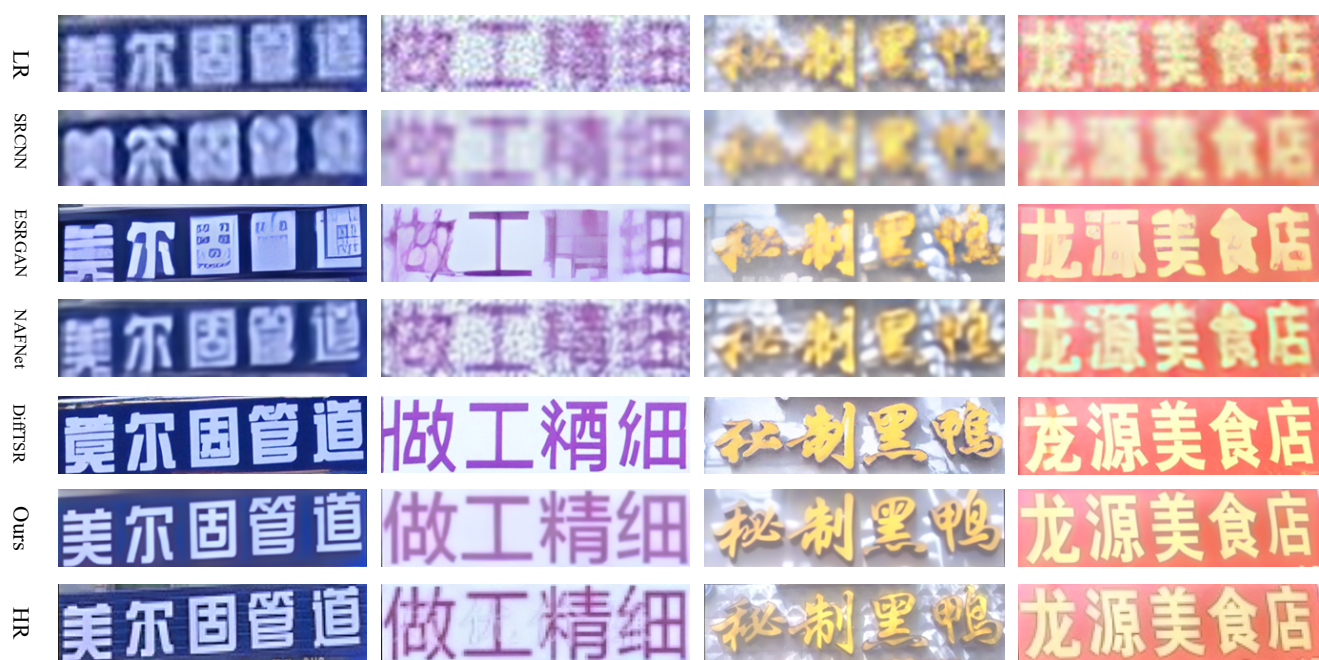


Figure 9. Qualitative comparison on the synthetic dataset with different methods including SRCNN [6], NAFNet [5], ESRGAN [36], the existing SOTA method DiffTSR [47] and our method for  $\times 4$  super-resolution.